## Conclusions

Although operational details have not been worked out, the AMAPS concept seems feasible and should result in significant reduction in deployment hardware and cost in many cases. Quantitative results are limited, but those obtained indicate axis transformation is easily accomplished before the first apogee. Furthermore, the discrete parameter model method seems to perform well for simple dissipation mechanisms.

## References

[1] Likins, P. W. and Bouvier, H. K., "Attitude Control of Nonrigid Spacecraft," *Astronautics and Aeronautics*, Vol. 9, No. 5, May 1971, pp. 64–71.

[2] Bracewell, R. N. and Garriott, O. K., "Rotation of Artificial Earth Satellites," *Nature*, Vol. 182, No. 4638, Sept. 20, 1958, pp. 760–762.

[3] Fitzgibbon, D. P. and Smith, W. E., "Final Report on Study of Viscous Liquid Passive Wobble Dampers for Spinning Satellites," EM 11-14, June 1960, TRW Systems, Space Technology Lab., Redondo Beach, Calif.

[4] Kaplan, M. H. et al., "Dynamics and Control for Orbital Retrieval Operations Using the Space Shuttle," KSC-TR-1113, Vol. I, May 1971, NASA, pp. 175–201.

[5] Thomson, W. T. and Reiter, G. S., "Attitude Drift of Space Vehicles," *Journal of the Astronautical Sciences*, Vol. 7, No. 2, 1960, pp. 29–34.

[6] Meirovitch, L. and Nelson, H. D., "On the High-Spin Motion of a Satellite Containing Elastic Parts," *Journal of Spacecraft and Rockets*, Vol. 3, No. 11, Nov. 1966, pp. 1597–1602.

[7] Hazeltine, W. R., "Passive Damping of Wobbling Satellites: General Stability Theory and Example," *Journal of the Aerospace Sciences*, Vol. 29, No. 5, May 1962, pp. 543–549, 557.

[8] Baines, D. J., "A Satellite Rotational Kinetic Energy Dissipator," *Journal of Spacecraft and Rockets*, Vol. 6, No. 7, July 1965, pp. 850–853.

[9] Thomson, W. T., *Introduction to Space Dynamics*, Wiley, New York, 1961, pp. 111–113.

[10] Meirovitch, L., *Methods of Analytical Dynamics*, McGraw-Hill, New York, 1970, pp. 72–79.

JUNE 1972 J. SPACECRAFT VOL. 9, NO. 6

# Pressurized Crack Behavior in Two-Dimensional Rocket Motor Geometries

E. C. FRANCIS*
*United Technology Center, Sunnyvale, Calif.*
AND
G. H. LINDSEY†
*Naval Postgraduate School, Monterey, Calif.*
AND
R. R. PARMERTER‡
*University of Washington, Seattle, Wash.*

**A method is presented for evaluating two-dimensional crack behavior in rocket motor geometries for pressure loadings in which the pressure is applied directly to the crack surfaces. The experimental requirements associated with pressurizing the crack necessitated the application of pressure over the two-dimensional plane surface of the specimen. Analytical solutions are developed which include the side pressure and relate the stress intensity factors to the classical unpressurized situation. Stress intensity factors for the complex cracked rocket motor geometries were evaluated using finite element computer techniques based on strain energy methods. Comparison between analytical predictions using elastic fracture mechanics and experimental observations of a brittle epoxy was quite good for the three different geometries tested. The work has application in fracture analysis of solid propellant rocket grains and in pressure vessels containing partial-thickness cracks which emanate from the inside.**

## Nomenclature

$A,B,C$ = star tip crack identification
$a,b$ = internal, external grain radius
$D$ = multiplicative factor
$E$ = Young's modulus
$G$ = general geometric function
$h$ = outside case radius
$K_I$ = stress intensity factor
$p$ = pressure
$r$ = radius
$u$ = displacement
$U$ = strain energy
$\gamma$ = surface energy
$\Delta$ = increment
$\delta_{ij}$ = Kronecker delta
$\theta$ = angle
$\nu$ = Poisson's ratio
$\sigma$ = stress

*Subscripts and Superscripts*

$a,b,c,d,e,f$ = problem identification
$i,j,k$ = tensor coordinates

Received June 16, 1971; revision received January 31, 1972. This work was supported by the Air Force Rocket Propulsion Laboratory, Edwards, Calif., under Contract F04611-69-C-0034. The authors wish to acknowledge the assistance of N. D. Walker Jr. in obtaining numerical solutions.

Index categories: Solid and Hybrid Rocket Engines; Computer Technology and Computer Simulation Techniques; Structural Static Analysis.

* Head, Propellant Properties Evaluation.
† Associate Professor of Aeronautics.
‡ Associate Professor of Aeronautics and Astronautics.

## Introduction

THE influence of cracks upon the structural integrity of solid propellant rocket motors constitutes a vital input to the design and reliability analyses. A necessary element in making crucial decisions of this nature is the dependability of the theory by which the motor is analyzed. Although cracks which occur in rocket motors have three-dimensional geometries and stress fields, and the propellant material in which they are embedded may exhibit nonlinear viscoelastic mechanical behavior, it is appropriate to first study two-dimensional motor geometries fabricated from linear materials to assess the accuracy and effectiveness of the fracture theory for the pressurization loading condition of an encased rocket grain. A knowledge of the performance of the theory for this problem will provide an important step in an orderly progression to the three-dimensional problem with real propellant material behavior.

Two significant contributions of the work are 1) the generation of an experimental method whereby crack surfaces can be pressure-loaded in a manner duplicating actual motor environments for three geometries and 2) the associated theoretical treatment required to interpret the experimental test results. Several specific applications of fracture mechanics are presented where predictions of crack instability in complex geometries were made and the theory was evaluated by experiment.

## Experimental Testing and Techniques

The material selected for study was a brittle epoxy, PLM-4B, manufactured by Photoelastic Inc. The geometries used were encased circular disks containing three different center perforations common to rocket grains as shown in Fig. 1. The sample preparation technique was to cast large cylindrical sections of the epoxy and machine the outside diameter to 7 in. Thin slices were sawed from the cylinders and milled to a thickness of 0.250 in. The inside perforation was machined using a router with a template of the correct geometry. The outside diameters of the grains and the inside diameters of Plexiglas cases were controlled to provide an approximate bonding clearance of 0.050 in. The grains were bonded in the cases with an epoxy adhesive (EPON-828/Versamid 125) and were cured at 72°F for 24 hr to minimize shrinkage.

In preparation for pressure testing, a small crack was inserted at the inner perforation of each case-bonded grain. The cracks were wedged with a sharp knife and hammer to a length of 0.25 to 0.50 in. long. Operator finesse was required to avoid the propagation of long cracks and the resulting loss of sample.

Pressure tests were performed in a pressure chamber (Fig. 2) designed especially for the disks. O-ring seals on the sides of the plastic case permitted the case to deform radially. Internal pressure was applied by a high-pressure nitrogen bottle through a regulator, and the pressure was increased very slowly while the sample was monitored through the Plexiglas windows of the pressure chamber. Backlighting was used to enhance detection of crack initiation, and the pressure which caused the crack to propagate was recorded. Pressure test results for the epoxy grains are presented in Table 1.

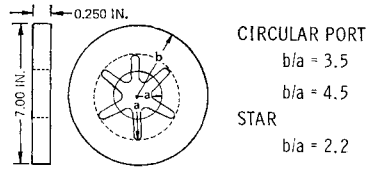


**Fig. 1 Epoxy grains before case bonding.**

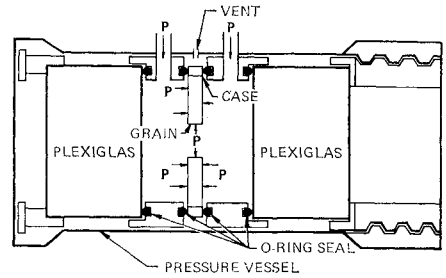


**Fig. 2 Pressurization test equipment.**

**Table 1 Pressure test results for epoxy grain slices[a]**

| Grain geometry | Pretest crack length, in. | Crack propagation pressure, psig |
|---|---|---|
| Circular port $b/a = 3.5$ | 0.45 | 215 |
| | 0.49 | 380 |
| | 0.70 | 215 |
| Circular port $b/a = 4.5$ | 0.40 | 365 |
| | 0.50 | 360 |
| | 0.61 | 250 |
| Star grain | 0.20 | 250 |
| | 0.30 | 210 |
| | 0.33 | 275 |

[a] All tests were run at 76° F.

Pressure levels at crack initiation varied from 210 to 380 psi. The pressure field inside the pressure vessel was applied at the bore surface, at the crack surface, and on the faces of the grain (as in an actual rocket motor application).

Upon propagating, the crack trajectory went straight to the case for the pressure-loaded epoxy grains. This was also observed for the star designs, which had initial crack angles of 30° from the star tips. A typical star grain after application of pressure is shown in Fig. 3. This particular grain was tested initially with a 0.120-in. crack at the star tip (identified as A). After it propagated at 250 psi, another crack (0.29 in. long) was inserted at B which subsequently propagated at 130 psi.

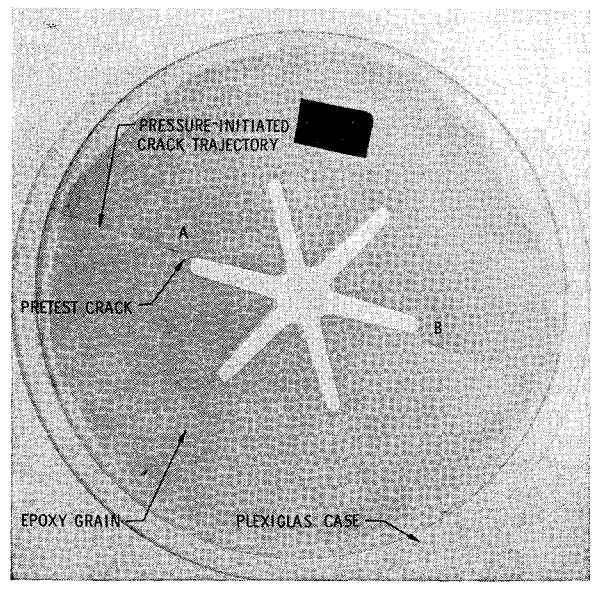


**Fig. 3 Trajectory of pressure-tested star epoxy grains.**

## Effect of Face Pressure on Plane Stress Pressurization Analysis

The presence of pressure over the face of the two-dimensional grain slice, resulting from the experimental requirements of pressurizing the crack, modifies the stress field from that of plane stress, i.e., with bore pressure only. Since calculation methods for finding $K_I$ in a thin slice deal with plane loadings, it is necessary to modify plane stress solutions to account for the face pressure.

### Exact Analysis Based on Superposition Principle

The stresses, $\sigma_{ij}$,[2] which arise in the problem with side pressure can be simply related to the stresses, $\sigma_{ij}$,[1] calculated from a plane stress problem through the use of the superposition principle.

The basic approach, which is similar to the development by Holsapple et al.[1] for thermal problems, is to divide each problem into subproblems that can be analyzed exactly with only one exception in each case. The exceptions which cannot be analyzed turn out to be identical for the two problems, and this provides the necessary link between $\sigma_{ij}^1$ and $\sigma_{ij}^2$.

First, consider the plane stress problem as a guide to the solution of interest. The solution $\sigma_{ij}^1$ can be obtained by superimposing the solutions to subproblems a), b), and c), as shown in Fig. 4. Problem a) is the grain alone, loaded in plane stress and having uniform pressure $p$ on the inner and outer boundaries. Problem b) is a case having the same internal pressure $p$. Problems a) and b) are stress compatible but are not displacement compatible, and the displacements of the deformed grain and case will differ by some amount, $\Delta u$.[1]

The solution to problem a) is a classical result

$$\sigma_{ij}^{(a1)} = -p\delta_{ij} \qquad i,j = 1,2 \qquad \sigma_{3k}^{(a1)} = 0 \qquad k = 1,2,3 \quad (1)$$

The constant stress field produces a constant strain field from which the displacement at the outer boundary $r = b$, is found from the axisymmetric equation

$$u^{(a1)} = -bp(1-\nu)/E \quad (2)$$

For the ring under uniform internal pressure, the radial displacement is

$$u^{(b1)} = pb^2/E_c h \quad (3)$$

The disparity in displacements is given by the difference between Eqs. (2) and (3)

$$\Delta u^{(1)} = u^{(b1)} - u^{(a1)} \quad (4)$$

Since the two-dimensional hydrostatic load of problem a) deforms the body into a geometrically similar shape, the outer boundary remains circular, and $\Delta u^1$ is independent of the angle $\theta$, even when the inner bore is of arbitrary shape. The case obviously remains circular. All irregularities of shape and the shear interactions between case and grain arise in the pullback problem c).

The pullback problem cannot be solved exactly for an arbitrary shape. However, within the limitations of the linear theory of elasticity it is known that the stresses, $\sigma_{ij}^{(c1)}$, in the pullback problem are linearly proportional to the magnitude of the pullback.

$$\sigma_{ij}^{(c1)} = \Delta u^{(1)} f(r,\theta) \quad (5)$$

where $f(r,\theta)$ is the solution for unit pullback. By superposition of these subproblems, the stress in the plane stress grain is

$$\sigma_{ij}^{(1)} = \Delta u^{(1)} f(r,\theta) - p\delta_{ij} \qquad i,j = 1,2 \qquad \sigma_{3k}^{(1)} = 0 \quad k = 1,2,3 \quad (6)$$

The problem with face pressure can be reduced similarly to a pullback problem by decomposition, as shown in Fig. 5. The solution for the hydrostatically pressurized grain is

$$\sigma_{ij}^{(d2)} = -p\delta_{ij} \qquad i,j = 1,2,3 \quad (7)$$

For this portion the strains are constant, and the displacements are given by the axisymmetric equations. The displacement at the outer boundary, $r = b$, is

$$u^{(d2)} = -bp(1-2\nu)/E \quad (8)$$

The case displacement is the same as Eq. (3); that is, $u^{(e2)} = u^{(b1)}$. The magnitude of the pullback in this instance has changed due to the $\sigma_{33}$ stress component in problem d).

$$\sigma_{ij}^{(f2)} = \Delta u^{(2)} f(r,\theta) \qquad \Delta u^2 = u^{(b1)} - u^{(d2)} \quad (9)$$

The stress for a unit pullback, $f(r,\theta)$, is the same as Eq. (5). The stress $\sigma_{ij}^{(2)}$ is obtained by superimposing the subproblems, as before.

$$\begin{aligned} \sigma_{ij}^{(2)} &= \Delta u^{(2)} f(r,\theta) - p\delta_{ij} \qquad i,j = 1,2 \\ \sigma_{33}^{(2)} &= -p \\ \sigma_{3k}^{(2)} &= 0 \qquad k = 1,2 \end{aligned} \quad (10)$$

Thus, for the in-plane stresses

$$\sigma_{ij}^{(1)} + p\delta_{ij} = \Delta u^{(1)} f(r,\theta) \quad (11)$$

$$\sigma_{ij}^{(2)} + p\delta_{ij} = \Delta u^{(2)} f(r,\theta) \quad (12)$$

Dividing the two equations

$$\frac{\sigma_{ij}^{(1)} + p\delta_{ij}}{\sigma_{ij}^{(2)} + p\delta_{ij}} = \frac{\Delta u^{(1)}}{\Delta u^{(2)}} = \frac{(1-\nu) + (E/E_c)(b/h)}{(1-2\nu) + (E/E_c)(b/h)} = D \quad (13)$$

The right-hand side of Eq. (13) is constant and constitutes a multiplicative factor $D$ which relates the two stress fields; thus $D$ can easily be calculated. If the solution to the problem a) with no face pressure is known, the solution to the experimental problem with face pressure can be found.

$$\sigma_{ij}^{(2)} + p\delta_{ij} = [\sigma_{ij}^{(1)} + p\delta_{ij}]/D \quad (14)$$

## Evaluation of Stress Intensity Factors

The solution to the plane stress problem without side load in the vicinity of the crack tip will have the form[2]

$$\sigma_{ij}^{(1)} = [K_I^{(1)}/(2r)^{1/2}]G_{ij}(\theta) \quad (15)$$

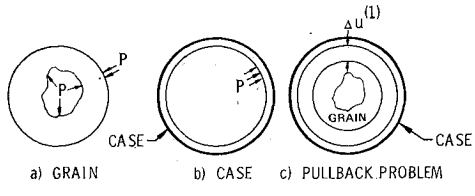


**Fig. 4 Superposition of pressure load problem.**

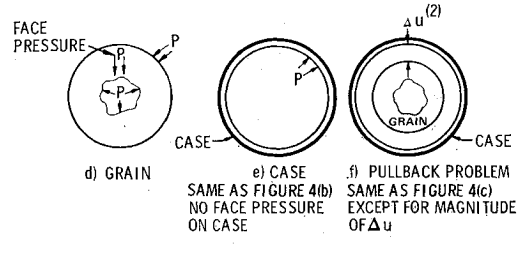


**Fig. 5 Superposition of side load on grain.**

Table 2 Side pressure parameters

| $\nu$ | 0.500 | 0.495 | 0.490 |
|---|---|---|---|
| $D$ | 44.2 | 23.4 | 16.1 |

If face pressures are added, the solution for the crack tip is

$$\sigma_{ij}^{(2)} = [K_I^{(2)}/(2r)^{1/2}]G_{ij}(\theta) \quad (16)$$

From the analogy given in Eq. (14) between plane stress and plane stress with face pressure

$$\frac{K_I^{(2)}}{(2r)^{1/2}} G_{ij} + p\delta_{ij} = \frac{[K_I^{(1)}/(2r)^{1/2}]G_{ij} + p\delta_{ij}}{D} \quad (17)$$

Near the crack tip the added term $p$ is negligible. Therefore

$$K_I^{(2)} = K_I^{(1)}/D \quad (18)$$

Thus, if the stress intensity factor is known for plane stress loading conditions, it can be determined for plane stress plus side pressure loading.

For an epoxy grain of 3.5-in. radius with Plexiglas case of 0.310-in. wall thickness, the $D$ value becomes 1.02. Thus, the effect of side pressure on $K_I$ is insignificant for the epoxy grain. The crack in the experimental tests with face pressure will propagate at virtually the same pressure calculated for plane stress; however, if the grain material is a soft elastomer, such as solid propellant with $E = 600$ psi and $\nu = 0.50$, the same geometry and case makes $D = 44.2$. $D$ values as a function of Poisson's ratio for $E = 600$ are shown in Table 2.

Therefore, low-modulus propellant behavior is very sensitive to the applied side load, and $D$ is very sensitive to small variations in Poisson's ratio.

## Material Properties

The material properties needed for a fracture analysis of the pressurized grain are modulus and Poisson's ratio for the grain and case, and fracture toughness for the grain material.

Modulus and Poisson's ratio were determined from uniaxial tensile tests with four strain gages on each sample. Test samples had two vertical gages for modulus evaluation and two horizontal gages for Poisson's ratio determination. Back-to-back strain gages were used to correct for specimen bending, and consistent results were produced. Sixteen tensile tests were conducted at 76°F by straining each sample to 2000 psi. The stress-strain curves were linear and were used for evaluation of Young's modulus.

Epoxy fracture toughness and surface energy determinations were made using a single-edge-crack tension specimen which is used extensively in metal fracture work.[3] Twelve such samples were tested in tension at 76°F. Specimens were 1 in. wide by 5 in. long by 0.25 in. thick. A small crack approximately 0.250 in. long was inserted from one side at the center of the specimen. All cracks were sawed and then wedged open to produce sharp natural crack tips. Measured material properties for the epoxy and Plexiglas are presented in Table 3, and the test data for the 12 epoxy fracture tests are presented in Table 4.

Table 3 Summary of material properties

| | PLM-4B epoxy | Plexiglass |
|---|---|---|
| Modulus, psi | 600,000 | 400,000 (slight relaxation) |
| Poisson's ratio | 0.347 | 0.33 |
| Surface energy, in.-lb/in.$^2$ | 0.250 | .. |
| Fracture toughness, psi-in.$^{1/2}$ | 542.4 | .. |

Table 4 Fracture toughness and surface energy data for PLM-4B epoxy at 76°F[a]

| Crack length, in | $KI_c$, psi (in.)$^{1/2}$ | $\gamma$, lb-in./in.$^2$ |
|---|---|---|
| 0.20 | 616 | 0.316 |
| 0.25 | 493 | 0.202 |
| 0.23 | 473 | 0.186 |
| 0.26 | 606 | 0.306 |
| 0.25 | 516 | 0.222 |
| 0.60 | 497 | 0.206 |
| 0.22 | 555 | 0.257 |
| 0.25 | 544 | 0.247 |
| 0.20 | 574 | 0.274 |
| 0.23 | 383 | 0.122 |
| 0.22 | 549 | 0.251 |
| 0.28 | 703 | 0.411 |
| | Average = 542.4 | 0.250 |
| | Standard deviation = 79.8 | 0.0704 |

[a] All samples were prepared from cast 0.250 in. epoxy sheets; samples were 1.00 in. wide.

### Evaluation of Grain Stress Intensity Factors

The onset of crack propagation was predicted by comparing the anticipated intensity factor $K_I$ with the fracture toughness value $K_{Ic}$. The predicted $K_I$ for the pressurized plane stress cracked epoxy grains was evaluated using numerical analysis procedures. $K_I$ was calculated from the strain energy release rate, $dU/dA$, using the plane stress equation of Irwin[4]

$$K_I^2 = E(dU/dA) \quad (19)$$

where $A$ is the crack surface area to be released, and $U$ is the total strain energy of the configuration. $K_I$ was evaluated numerically for the two circular port geometries ($b/a = 3.5$ and 4.5) and the six-pointed-star design for different crack lengths. The Rohm and Haas[5] finite element program was used for the grain calculations. The mesh system for one of the circular port grains (with a crack depth of 1.00 in.) is shown in Fig. 6. The basic Rohm and Haas computer code was modified to calculate the total strain energy in the grain, and strain energy release rates were determined from two successive calculations of $U$ with a 0.050-in. change in crack length. A relatively coarse grid was used following the suggestion of Deverall and Lindsey[6] who made a comparative study with classical solutions to show that fine grids were not necessarily required for good accuracy in determining $K_I$ if the strain energy release rate method is utilized.

Results of the analysis of the two-dimensional grain slice pressure tests for $K_I$, using plane stress numerical calculations, are presented in Fig. 7. These $K_I$ curves have a correction factor of 0.98 to account for the pressure on the grain sides. The relative positions of the curves in Fig. 7 are due to the

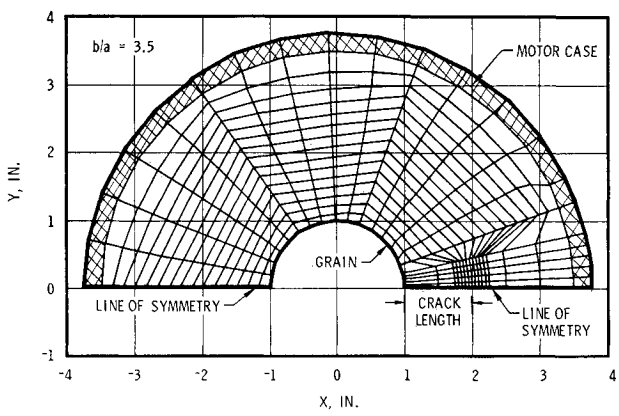


Fig. 6 Typical mesh for finite element computer analysis.

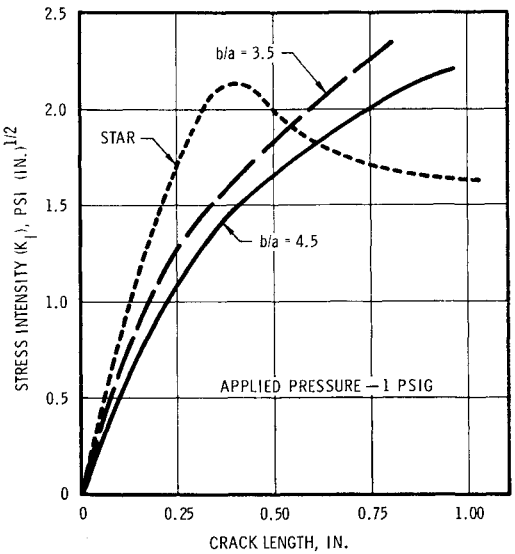


**Fig. 7 Stress intensity factors vs crack length.**

epoxy grains having moduli of the same order of magnitude as the cases. For low-modulus grains, the $K_I$ curve for the circular port grains with a $b/a$ ratio of 4.5 would be above the curve for the grain having a $b/a$ ratio of 3.5.

## Comparison of Theory and Experiment

The total $K_I$ value in the pressurized grain consists of the component generated by the pressurization condition plus the component generated by the shrinkage of the epoxy adhesive used to bond the grain to the Plexiglas case. During the cure process the adhesive changed volume after becoming solid. The cure shrinkage after gel for typical epoxies is 3%. Numerical analysis showed that 99% of the grain pressurization load was absorbed by the high-modulus epoxy grain. One percent of the pressure load was supported by the Plexiglas case. Therefore, the adhesive shrinkage would tend to load the case rather than deform the stiff grain, and only 1% of the cure shrinkage after gel would contribute to loading the grain. This shrinkage loading is insignificant for the high-modulus epoxy grain.

Analysis of the grains using the numerically evaluated stress intensity factors proceeded by obtaining from Fig. 7 the $K_I$/unit load for the appropriate crack length in each grain. Multiplying by the test pressure at fracture, the $K_I$ values for each test were compared with the allowable fracture toughness values shown in Fig. 8. All of the pressurized grain fractures fell within the 2 $\sigma$ variation of measured epoxy $K_{Ic}$ values. These results were taken as confirmation of the energy analysis methods, and they provide a measure of the accuracy of the theory for grain fracture analysis of

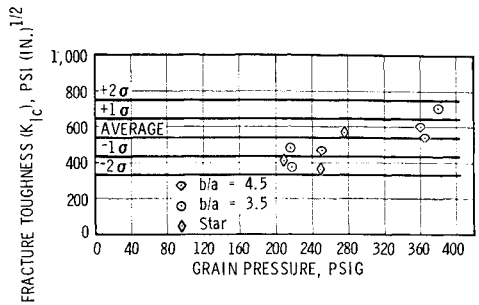


**Fig. 8 Comparison of epoxy grain pressure test results with fracture toughness.**

idealized geometries and materials. Direct applications of the work can be made to a variety of rocket motor and pressure vessel problems.

## Conclusion

Motivated by the need to analyze flaw behavior in rocket motor solid propellant grains, predictions of crack instability using fracture mechanics have been substantiated by experiment for two-dimensional geometries. With the analogy between pressurized plane stress and classical plane stress, it has been possible to develop a bonafide test method for performing experiments on pressurized cracks in bonded rocket geometries with arbitrary inner perforations. Test analyses with solid propellants will require consideration of viscoelastic effects.

## References

[1] Holsapple, K. A., Schmidt, W. F., and Fourney, M. E., "Some Pressure-Temperature Equivalences in Elasticity with Application to Case-Bonded Solid Propellant Rocket Grains," *Journal of Applied Mechanics*, Vol. 37, No. 4, Dec. 1970, pp. 1158–1160.

[2] Sih, G. C., and Liebowitz, H., "Mathematical Theories of Brittle Fracture," *Fracture, an Advanced Treatise*, Vol. II, Academic Press, New York, 1968, pp. 67–190.

[3] Brown, W. F., and Srawley, J. E., "Plane Strain Crack Toughness Testing of High Strength Metallic Materials," Publication 410, 1967, American Society for Testing Materials, Philadelphia, Pa. p. 12.

[4] Irwin, G. R., "Analysis of Stresses and Strains Near the End of a Crack Traversing a Plate," *Journal of Applied Mechanics*, Vol. 24, Sept. 1957, p. 361.

[5] Becker, E. B., and Brisbane, J. J., "Application of the Finite Element to Stress Analysis of Solid Propellant Rocket Grains," S-76, 1966, Rohm and Haas Co., Redstone Research Divi., Huntsville, Ala.

[6] Deverall, L. I., and Lindsey, G. H., "A Comparison of Numerical Methods For Determining Stress Intensity Factors," *Journal of Engineering for Industry (ASME)*, to be published.